Molecular Cell, Vol. 17, 869–883, March 18, 2005, Copyright ©2005 by Elsevier Inc. DOI 10.1016/j.molcel.2005.02.016

Major Conformational Change in the Complex SF3b upon Integration into the Spliceosomal U11/U12 di-snRNP as Revealed by Electron Cryomicroscopy

Monika M. Golas, Bjoern Sander, Cindy L. Will, Reinhard Lührmann,* and Holger Stark*
Department of Cellular Biochemistry and Research Group of 3D Electron Cryomicroscopy
Max Planck Institute for Biophysical Chemistry
Am Faßberg 11
D-37077 Göttingen
Germany

Summary

In some eukaryotes, a minor class of introns is removed by the U12-dependent spliceosome, which contains the small nuclear ribonucleoprotein (snRNP) heterodimer U11/U12. The U11/U12 di-snRNP forms a molecular bridge that functionally pairs the intron ends of the pre-mRNA. We have determined the three-dimensional (3D) structure of the human U11/U12 di-snRNP by single particle electron cryomicroscopy using angular reconstitution and random conical tilt. SF3b, a heteromeric protein complex functionally important for branch site recognition, was located in the U11/U12 di-snRNP by antibody labeling and by identification of structural domains of SF3b155, SF3b49, and p14. The conformation of SF3b bound to the U11/U12 di-snRNP differs from that of isolated SF3b: upon integration into the di-snRNP, SF3b rearranges into a more open form. The manner in which SF3b is integrated in the U11/U12 di-snRNP has important implications for branch site recognition. Furthermore, a putative model of the pre-mRNA binding to the U11/U12 di-snRNP is proposed.

Introduction

The accurate excision of introns from eukaryotic pre-mRNA is essential for the correct translation of mature mRNA into proteins (Burge et al., 1999). In the first catalytic step of splicing, the branchpoint adenosine of the intron attacks the 5′ splice site, leading to the formation of a free 3′-OH group at the 3′ end of the 5′ exon. Subsequently, this 3′-OH attacks the 3′ splice site, leading to the formation of the mRNA and release of the intron. Splicing is catalyzed by a nuclear RNA–protein (RNP) complex termed the spliceosome. The major spliceosome is assembled on pre-mRNA by the sequential binding of the snRNPs U1, U2, and U4/U6.U5 as well as additional factors. In higher eukaryotes, a rare class of introns is spliced by the minor spliceosome that contains the U11/U12 di-snRNP and the U4atac/U6atac.U5 tri-snRNP (Patel and Steitz, 2003).

The assembly of the major spliceosome is initiated by the successive binding of the U1 and U2 snRNPs to the pre-mRNA, forming the A complex. In contrast, the U11 and U12 snRNPs form a stable U11/U12 di-snRNP that binds as a single entity to pre-mRNA during assembly of the minor A complex (Frilander and Steitz, 1999). In this complex, the U11 and U12 snRNAs bind cooperatively to the 5′ splice site and to the branch site of the pre-mRNA, respectively. Hence, the U11/U12 di-snRNP performs a very important bridging function, functionally pairing the intron ends in the first step of spliceosome assembly.

The U11 and U12 snRNAs make up ~7% of the di-snRNP's total mass of ~1.2–1.3 MDa. These snRNAs contain the Sm consensus sequence $RAU_{4-6}GR$ to which the Sm proteins bind. In addition, the human U11/U12 di-snRNP contains the protein complex SF3b, seven unique proteins, and three proteins found in the major spliceosome (Will et al., 1999, 2001, 2004). SF3b contributes a molecular mass of ~450 kDa; it consists of the seven proteins SF3b155, SF3b145, SF3b49, SF3b14a (also termed p14), SF3b14b, and SF3b10 (Das et al., 1999; Krämer et al., 1999; Will et al., 2001, 2002) plus the substoichiometric DEAD-box protein SF3b125, which is not present in the fully assembled snRNPs (Will et al., 2002).

A comparison of the protein compositions of the U2 and U11/U12 snRNPs revealed that both particles share all SF3b proteins (Will et al., 1999). SF3b has been demonstrated to play a key role in the recruitment and tethering of the U2 snRNP to the intronic branch site. Most of the SF3b proteins crosslink to pre-mRNA in a region spanning ~25 nucleotides upstream and ~5 nucleotides downstream of the branchpoint (Champion-Arnaud and Reed, 1994; Gozani et al., 1996, 1998; MacMillan et al., 1994). In the major spliceosome, p14 interacts directly with the branchpoint adenosine in the A complex and subsequent spliceosomal complexes, including the catalytically active C complex (Query et al., 1996; Will et al., 2001). In the minor spliceosome, SF3b is expected to play a similar role in the recognition of the branchpoint region. Therefore, localization of SF3b in the U11/U12 di-snRNP should direct us to a functionally important region of the subsequently formed minor spliceosome, namely those proteins potentially taking part in the first catalytic step of splicing.

Recently, the structure of isolated SF3b was determined by electron cryomicroscopy, allowing the positions of SF3b155, SF3b49, and p14 to be determined directly (Golas et al., 2003). The shape of purified SF3b resembles a bivalve shell, with p14 located inside the central cavity of the complex. The remarkable architecture of isolated SF3b, with p14 surrounded by cage-like density elements, raised the question of how p14 might bind the catalytically active branchpoint adenosine of the pre-mRNA. Two potential mechanisms can be envisioned. First, the conformation of SF3b could remain unchanged in the U11/U12 di-snRNP. Consequently, the pre-mRNA would have to thread through the outer SF3b shell to reach p14 in the inner cavity of SF3b. Second, SF3b could undergo conformational changes, making p14 accessible for pre-mRNA interaction without the need for a threading mechanism. To test these

*Correspondence: hstark1@gwdg.de (H.S.); reinhard.luehrmann@mpi-bpc.mpg.de (R.L.)

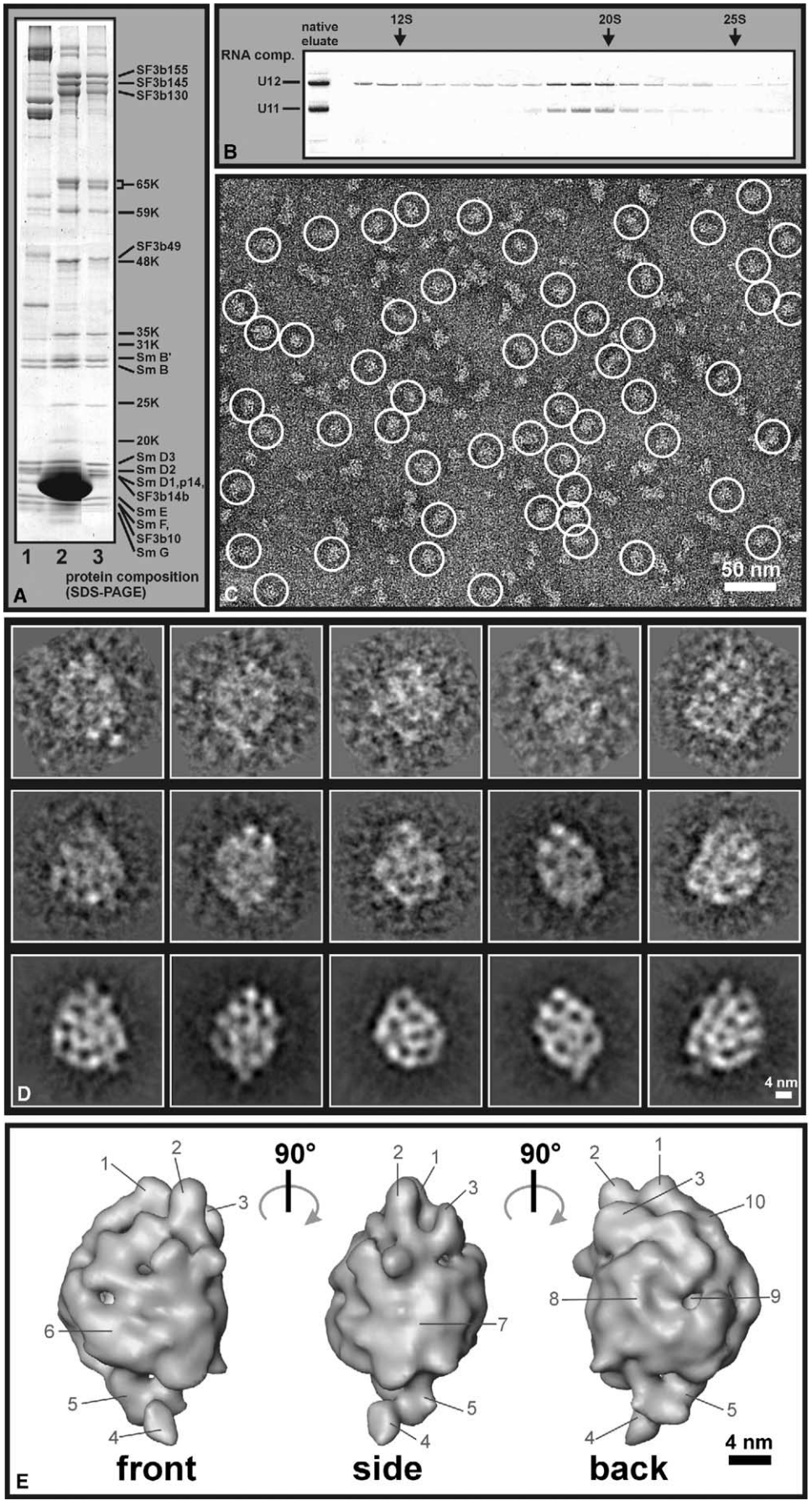
SF3b155
SF3b145
SF3b130
65K
59K
SF3b49
48K
35K
31K
Sm B'
Sm B
25K
20K
Sm D3
Sm D2
Sm D1,p14,
SF3b14b
Sm E
Sm F,
SF3b10
Sm G
1 2 3
protein composition
(SDS-PAGE)
A
native
eluate
12S
20S
25S
RNA comp.
U12
U11
B
50 nm
C
4 nm
D
90°
90°
1
2
3
4
5
6
7
8
9
10
front
side
back
4 nm
E

models, we have localized SF3b in the 3D U11/U12 di-snRNP structure determined by single-particle electron cryomicroscopy. The conformation of SF3b in the U11/U12 di-snRNP compared with isolated SF3b indicated that it has undergone a structural change. Our results provide first insights into a structural rearrangement that appears to be important for branch-site recognition and for the molecular architecture of early spliceosomal complexes.

Results

Approaches for Structure Determination of the U11/U12 di-snRNP

In this study, we present the 3D structure of the human U11/U12 di-snRNP by using a variety of experimental approaches (see flow chart in Figure S1 available with this article online). For structural analysis, U11/U12 di-snRNPs were affinity selected under native conditions by using a biotinylated 2′O-methyl-oligonucleotide and streptavidin agarose. The protein pattern of purified native U11/U12 di-snRNPs appeared to be identical to that of particles isolated under denaturing conditions; they contained all Sm proteins, the seven SF3b proteins, and other particle-specific proteins (Will et al., 1999, 2004) (Figure 1A). The majority of eluted particles remained intact, sedimenting as an 18S complex in glycerol gradients (Figure 1B). Only a small portion of U12 snRNA was detected in the lower molecular weight fractions (~12S). For structural analysis, the native U11/U12 di-snRNP was negatively stained by the double carbon-sandwich method and frozen in liquid nitrogen (Golas et al., 2003). The electron micrographs of native U11/U12 di-snRNPs exhibited a monodisperse population of slightly elongated globular particles with dimensions of 150–260 Å (Figure 1C).

The U11/U12 di-snRNP Structure Determined by Angular Reconstitution

Two independent data sets of the U11/U12 di-snRNP were imaged. Conditions for the first data set were chosen to give high contrast (recorded on a CCD camera, sample at room temperature), whereas conditions for the second set were designed to give maximum resolution for structure determination (recorded on film, sample at liquid nitrogen temperature).

From the first data set recorded on CCD camera, 2352 particle images were selected interactively, corrected for the contrast transfer function (CTF) (Sander et al., 2003a), and used to compute a 3D structure at ~25 Å resolution. Owing to the high contrast of the raw data, similarities between individual particle images (Figure 1D, top), class averages (middle row) consisting of three to ten class members, and reprojections (bottom row) of the 3D map are readily apparent. The surface representation of the U11/U12 di-snRNP revealed a globular particle with three major protuberances (nos. 1–3) located at the top and two protruding regions (nos. 4 and 5) at the bottom (Figure 1E).

This 3D structure was instrumental in establishing the overall size and gross morphological features of the particle, allowing more readily the manual selection of ~9000 intact, nonaggregated particles from the images recorded on film for the second data set. Of this second data set, a minor fraction of very small particles—probably representing fragments of the U11/U12 di-snRNP (cf. Figure 1B)—were not selected for image analysis. Projection angles of class averages from the second data set were determined de novo by angular reconstitution without using the 3D structure of the CCD camera data set as a starting model; thus, results from the two data sets provided independent confirmation of one another. During CTF correction, roughly 3% of all individual images were excluded on the basis of their low quality in average power spectra (Sander et al., 2003a). A gallery displaying filtered particles (Figure 2A, top), class averages with ~10–20 members (middle), and reprojections (bottom) demonstrates a wealth of details. Typical projections of the U11/U12 di-snRNP show globular particles with two protuberances at the bottom (e.g., third view). The resolution of the 3D map determined by the Fourier shell correlation (FSC) function (Harauz and van Heel, 1986) was 8.9 Å using the 5σ criterion, 10.4 Å using the 0.143 FSC criterion, and 13.4 Å using the 0.5 FSC value (Figure 2B). The Euler angle plot of all projection images revealed a distribution over the unit sphere that was nearly random with respect to latitude angles, whereas some preferred orientations were observed with respect to rotation about the particle's long axis (Figure 2C).

General Architecture of the Human U11/U12 di-snRNP

The surface representation of the U11/U12 di-snRNP is shown in Figure 2D. To emphasize the higher-resolution information, the 3D map was bandpass-filtered to 9–20 $Å^{-1}$. The boundary of the corresponding unfiltered surface encloses a molecular mass of ~1.3 MDa, consistent with the predicted mass (Will et al., 2004). The

Figure 1. Characterization of Native U11/U12 di-snRNP

(A) Protein composition of the U11/U12 di-snRNP. Lane 1 shows the input snRNPs (i.e., 18S gradient fractions), lane 2 affinity-purified U11/U12 di-snRNPs eluted under denaturing conditions (Will et al., 1999), and lane 3 U11/U12 di-snRNPs eluted under native conditions that were used for electron microscopy (EM).

(B) Silver-stained snRNA composition of the native U11/U12 di-snRNP eluate and of glycerol gradient fractions of the eluate. Purified U11/U12 di-snRNPs peaked at ~18S.

(C) EM field of native U11/U12 di-snRNPs showing a monodisperse population of elongated particles with a size of ~15–26 nm (white circles).

(D) Filtered, aligned single particle images (2-fold binned 1k × 1k CCD camera; top row), corresponding class averages (middle), and reprojections (bottom) are shown.

(E) Surface representation of the U11/U12 di-snRNP (CCD camera) depicted in three views at a resolution of ~25 Å. To facilitate orientation and comparison with Figures 2 and 3, characteristic topographical features ("landmarks") numbered 1–11 are introduced.

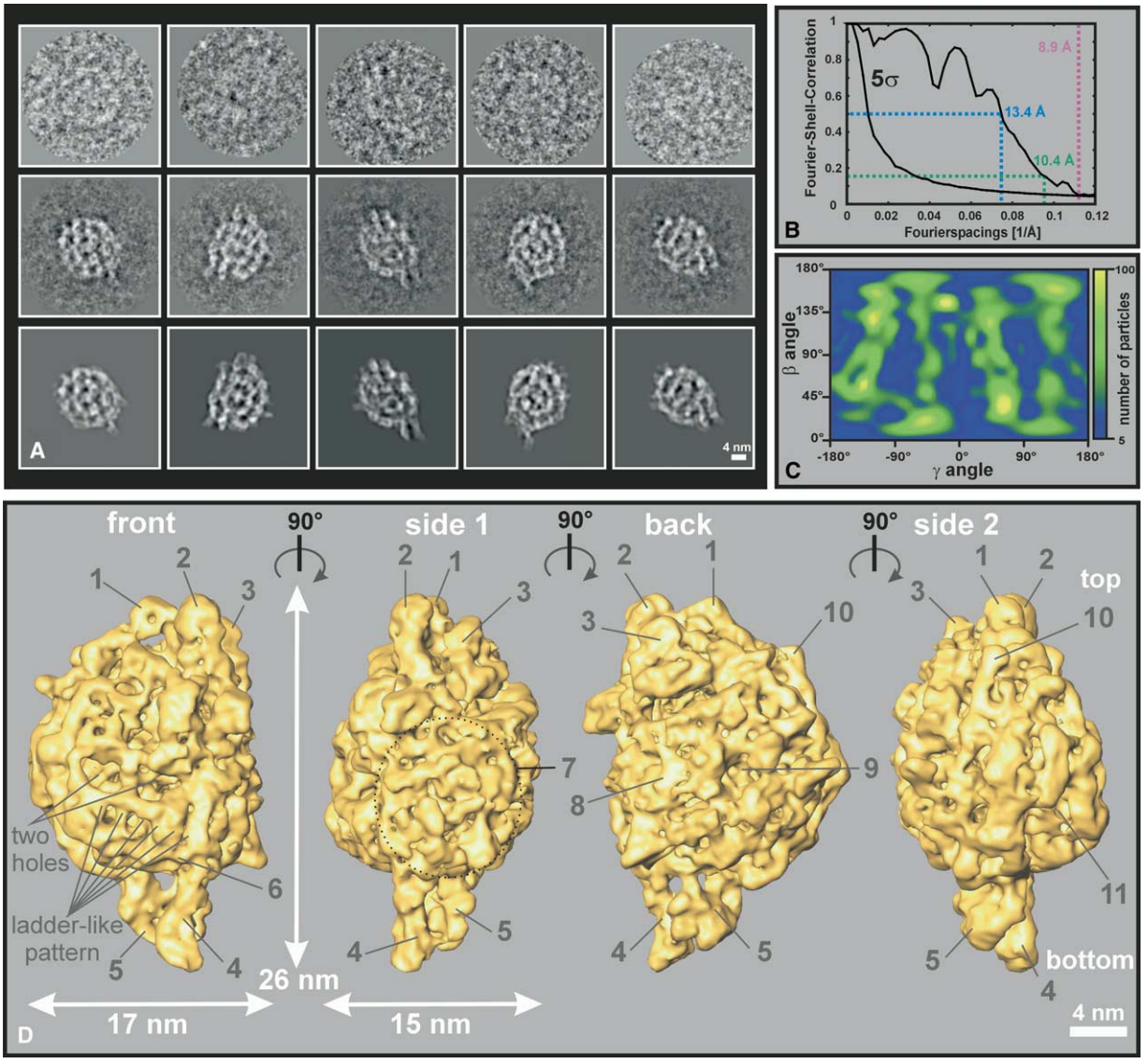

Figure 2. Angular Reconstitution of Native U11/U12 di-snRNP Taken on Film

(A) Gallery showing filtered single particles (top), class averages (middle), and reprojections (bottom) used to calculate the 3D structure in (D). Compared with the data set obtained with the CCD camera, the image contrast is much lower, but the resolution is higher.

(B) FSC plot of the 3D reconstruction. The resolution was found to be 8.9 Å (5σ threshold), 10.4 Å (0.143 FSC), and 13.4 Å (0.5 FSC).

(C) Distribution of projection angles of the 3D reconstruction showing the presence of a wide variety of different projection angles. Relative particle numbers per unit area are color coded as shown on the right (linear scale).

(D) Surface representation of the native U11/U12 di-snRNP. Numbering of characteristic landmarks is as in Figure 1E.

U11/U12 di-snRNP is a ~26 nm long globular particle with a width of 15–17 nm.

The upper region of the U11/U12 di-snRNP contains three protuberances (numbered 1–3 in Figure 2D). One side of the U11/U12 di-snRNP ("front") reveals two adjacent elongated pore-like holes, below which a ladder-like pattern can be discerned (see below). Two protruding elements are seen at the lower end and are mainly responsible for the somewhat elongated appearance of the complex. Of these, one (no. 4) is roughly straight, whereas the other (no. 5) is disc shaped with a central hole. Another view ("side 1") shows in the lower region of the particle a compact mass (no. 7; shown enclosed in a black dotted line) with a small, elongated hole in the middle. This mass is connected by thin bridges to the top of the complex. The "back" view reveals a deep cleft (no. 9) with a triangular density element in the middle of the cleft. Another view ("side 2") shows a prominent groove at the bottom with a globular domain located at the base of this groove (no. 11).

Random Conical Tilt Analysis and Determination of Handedness

3D maps obtained from zero-tilt images are ambiguous with respect to handedness. There are two methods to determine the handedness a posteriori: (1) by perform-

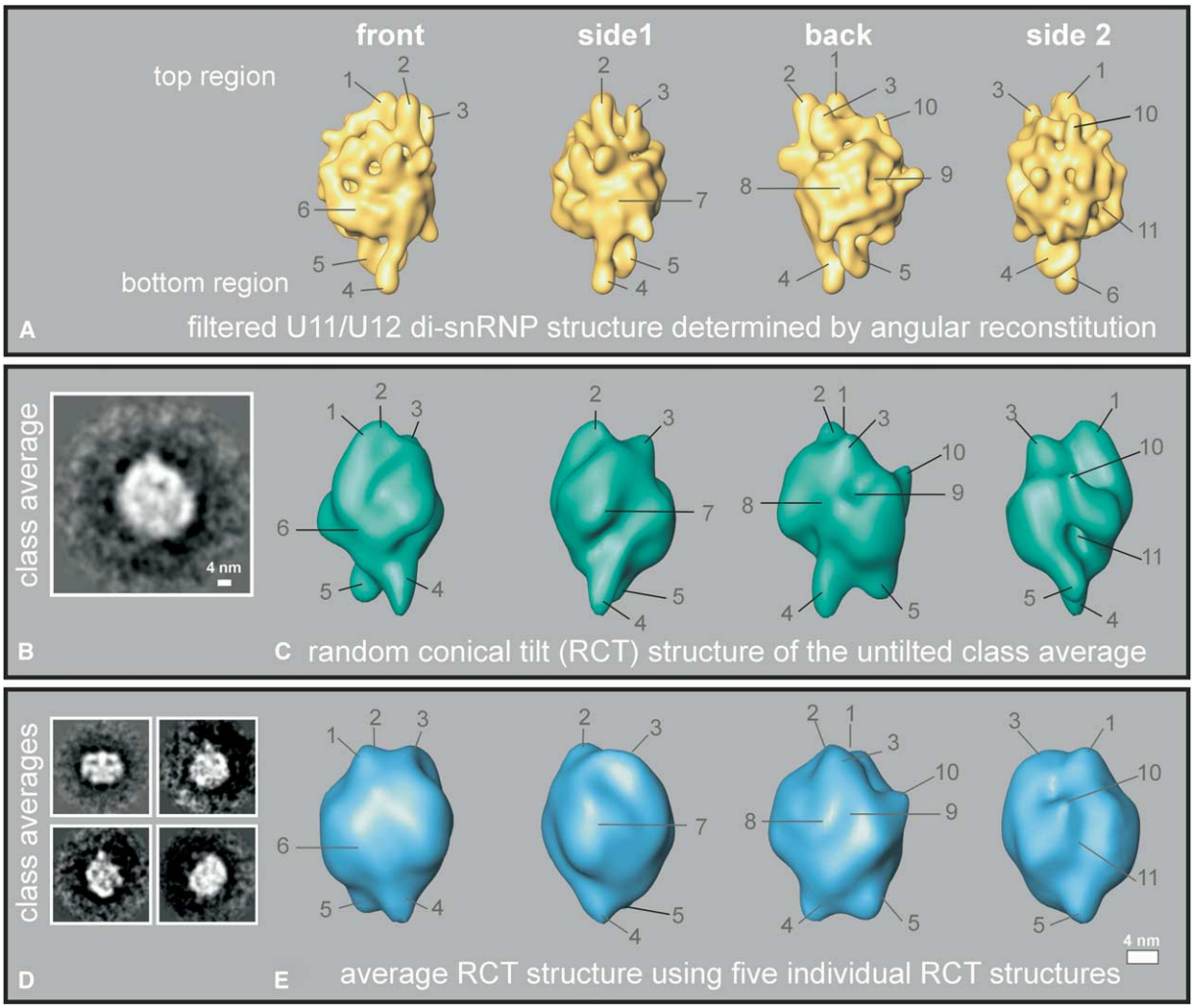

Figure 3. Random Conical Tilt Analysis of Native U11/U12 di-snRNP

(A) Lowpass-filtered surface representation of the U11/U12 di-snRNP as obtained by angular reconstitution (Figure 2D). Orientation and numbering of characteristic landmarks are as in Figures 1E and 2D.

(B) Class average of 47 untilted U11/U12 di-snRNPs used for random conical tilt (RCT).

(C) Surface representation derived from RCT (untilted class average in [B]). Comparisons with the lowpass-filtered U11/U12 di-snRNP structure calculated by angular reconstitution (A) show a similar general architecture, with a globular main body and two protuberances at the bottom. Note that RCT reconstructions are generally limited to low resolution for technical reasons.

(D) Selected class averages used together with the class in (B) to calculate an average RCT structure of the U11/U12 di-snRNP.

(E) Average RCT structure of the U11/U12 di-snRNP using five individual RCT structures.

ing tilt experiments such as random conical tilt (RCT; Radermacher, 1988) and (2) by fitting structures with known handedness (see below). Both methods were applied to determine the handedness of the U11/U12 di-snRNP.

One RCT structure and its untilted class average are presented in Figures 3B (class average) and 3C (surface view); for comparison, Figure 3A shows the structure as obtained in Figure 2D but lowpass filtered for easier comparison with the RCT-derived map. The combined 3D structure of the five largest classes (Figures 3B and 3D) is depicted in Figure 3E. By comparing the structures obtained by the two different reconstruction techniques (angular reconstitution in Figure 3A and RCT in Figures 3C and 3E), the handedness of the 3D map was determined. A comparison with the mirror image of Figure 3A showed no correspondence. Structural features such as the two protuberances at the bottom or the top of the particle were very similar in the 3D maps obtained from angular reconstitution and from RCT (compare numbered landmarks in Figures 3A, 3C, and 3E). Thus, RCT not only revealed the handedness of the U11/U12 particle, but it also provided an additional independent confirmation of the general architecture of the U11/U12 di-snRNP.

Location of Structural Elements of the First Shell Half of Isolated SF3b in the U11/U12 di-snRNP

SF3b comprises one-third of the total mass of the U11/U12 di-snRNP. It also represents a functionally impor-

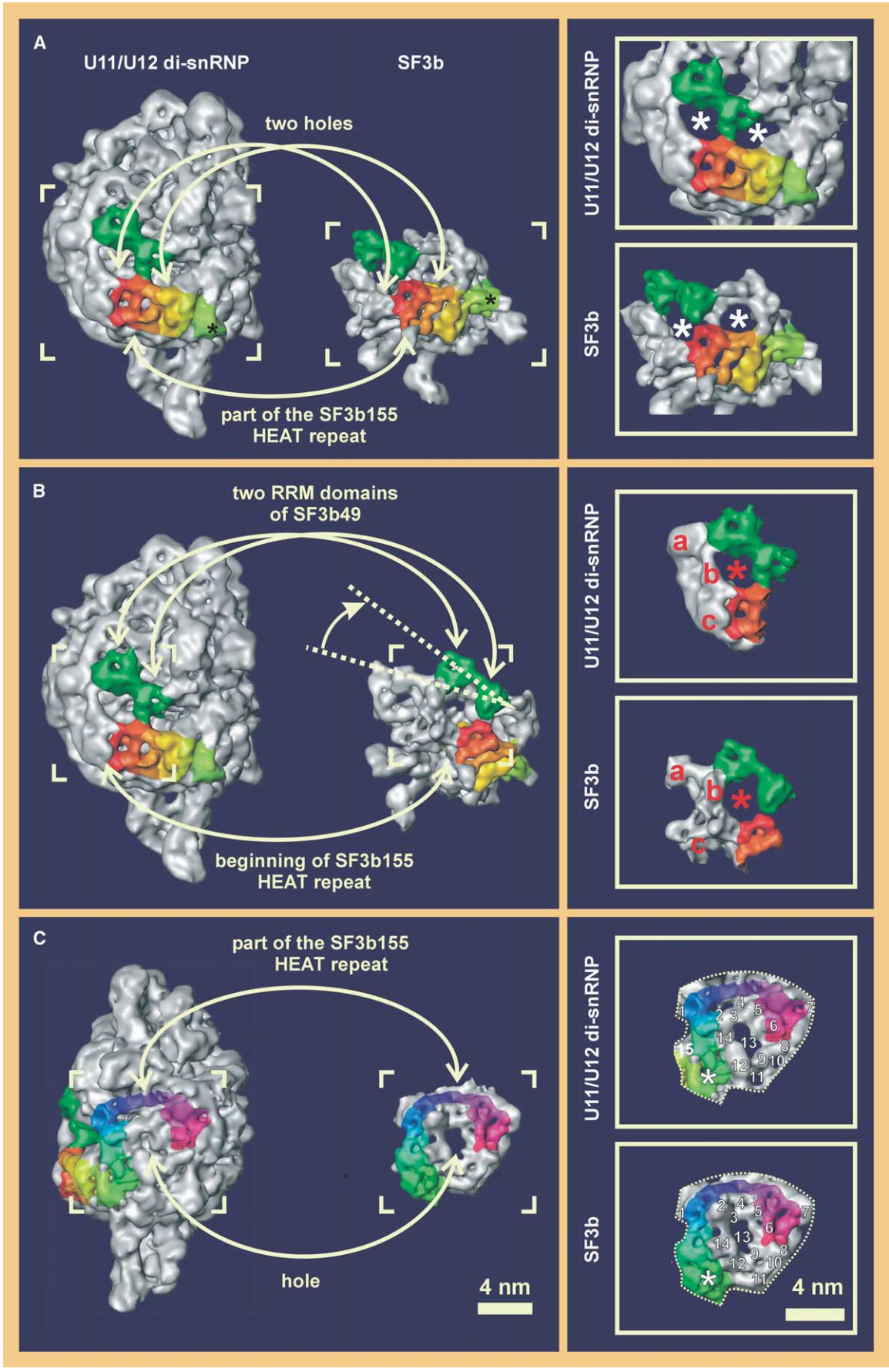
A
U11/U12 di-snRNP
SF3b
two holes
part of the SF3b155
HEAT repeat
U11/U12 di-snRNP
SF3b
B
two RRM domains
of SF3b49
beginning of SF3b155
HEAT repeat
a
b
c
U11/U12 di-snRNP
SF3b
C
part of the SF3b155
HEAT repeat
hole
4 nm
U11/U12 di-snRNP
SF3b
4 nm

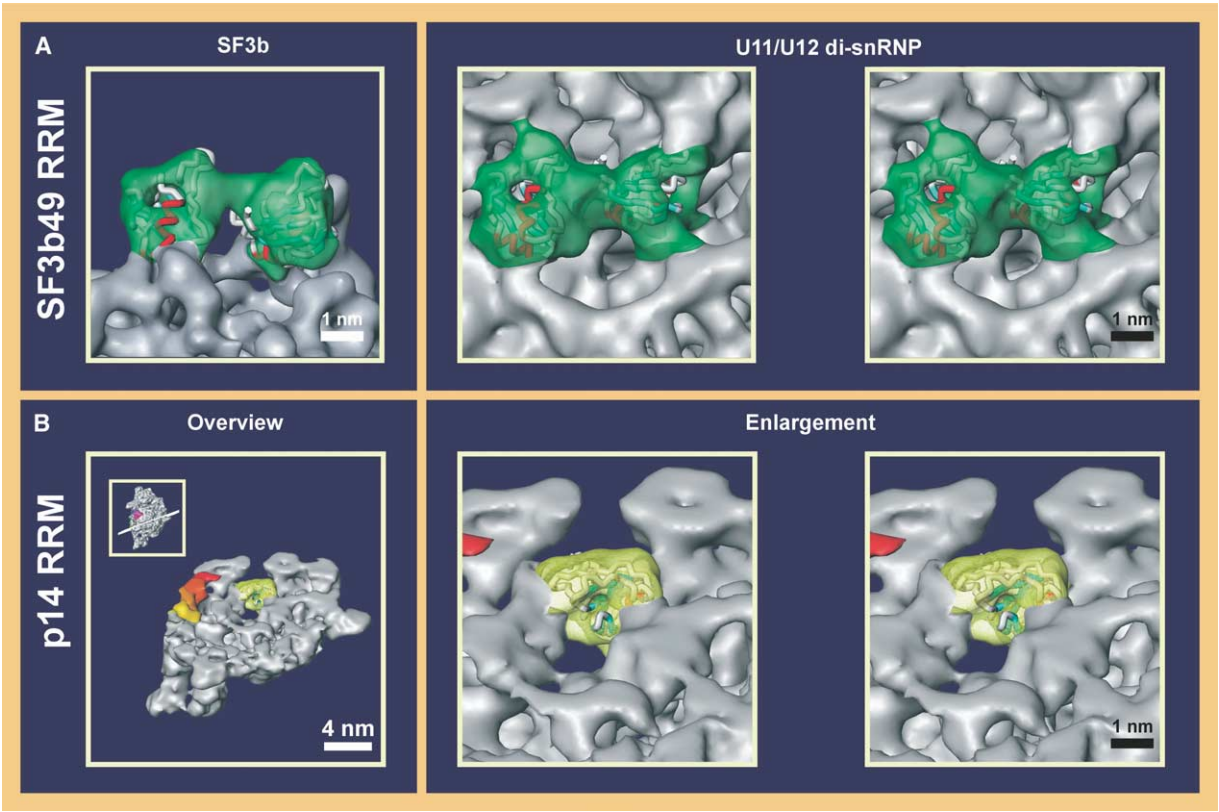

Figure 5. Fitting of Molecular Models of SF3b Proteins into the U11/U12 di-snRNP

(A) Fitting of the two adjacent RRMs of SF349 (green) into the isolated SF3b as reported in Golas et al. (2003) and in the U11/U12 di-snRNP in stereo view.

(B) Fitting of the p14 RRM into the U11/U12 di-snRNP. The cutaway view is shown in the orientation of the back view and tilted somewhat to enable the visualization of the p14 RRM (yellow). The inset on the left side shows the cutting plane. The enlarged version in stereo view reveals an excellent fit of the p14 RRM model and the yellow colored U11/U12 di-snRNP density.

tant region of the U11/U12 di-snRNP, which is thought to associate with the branch site region of the pre-mRNA in the spliceosome. The location of SF3b is therefore of central importance for the interpretation of the structure of the U11/U12 di-snRNP.

Structural domains have been predicted for three of the SF3b proteins, including the tandem helical HEAT repeats in SF3b155 (Wang et al., 1998) and the RNA recognition motifs (RRM) of SF3b49 and p14 (Champion-Arnaud and Reed, 1994; Will et al., 2001), which form four β strands and two α helices. In our recent study of isolated SF3b (Golas et al., 2003), the most regular parts of the HEAT motif became visible as a ladder-like pattern at a resolution below ~14 Å (according to the 5σ criterion), although without clear separation of the tandem helical pairs, which required a resolution of ~7–10 Å. Likewise, RRMs were identified in our previous study at ~7–10 Å resolution. In the U11/U12 di-snRNP, the HEAT repeats could also be detected: a row of seven parallel ordered columns, which are separated from each other, can be seen in the frontal view of the di-snRNP (Figure 4A, rainbow colors; for

Figure 4. Analysis of Structural Similarities between Isolated SF3b and the U11/U12 di-snRNP

In the left-hand panels, corresponding elements of the U11/U12 di-snRNP and isolated SF3b are linked with double-headed arrows. In the right-hand panels, close-up views are shown that correspond to the frame corners. For clarity, density located behind the fitted masses was removed in the close ups. The views are "front" and "side 1" from Figure 2D.

(A) Both complexes show a row of parallel columns (rainbow colors) that correspond to the N-terminal HEAT repeats of SF3b155. Above the HEAT repeats, two pore-like holes in the surface are located. The putative hinge region is labeled with a black asterisk. Close-up views with the characteristic holes (white asterisks) and the ladder-like HEAT repeats.

(B) As in (A) but emphasizing the two RNA recognition motif (RRM) domains of SF3b49 (green). The RRMs are rotated by 20° in the U11/U12 particle with respect to their orientation in isolated SF3b. The rotation angle is indicated in yellow.

(C) As in (A) and (B) but with rotation to show the second shell half of SF3b, which contains most of the SF3b155 HEAT repeats (rainbow colors) surrounding a small hole. Density elements 1–14 are described in the text. The contours of the SF3b shell half and its corresponding densities in the U11/U12 di-snRNP (close ups; yellow dotted line) are very similar.

description of the remaining part of HEAT repeats, see below). The column length varies between 30 Å and 40 Å, and the column-to-column distance is ~7 Å, which is consistent with results obtained earlier with isolated SF3b (Golas et al., 2003).

An additional prominent structural feature found in both SF3b and the U11/U12 di-snRNP is a pair of holes located directly above the tandem helical repeats (Figure 4A, white asterisks). In isolated SF3b, the SF3b49 RRMs are found above the first HEAT repeats as part of the wall of the left hole. In contrast to SF3b, the U11/U12 di-snRNP contains six proteins with predicted RRM domains, including SF3b49 (two adjacent RRMs), p14 (one RRM), 65K (two RRMs separated by a long stretch of amino acids [aa]), 35K (one RRM), 31K (one RRM), and Urp (one RRM). We analyzed the putative RRM domains according to (1) size (Figure S2), (2) mass (Figures S2 and S3), and (3) cross correlation coefficient (CCC) (Figures S4, S5, and S8–S10; Table S1). Some of the putative RRM domains were found in close proximity to one another and thus potentially represented the two adjacent SF3b49 RRMs. Fits of the SF3b49 RRM densities selected manually from the 3D map of isolated SF3b exhibited the highest CCC of 0.84 (Figure S4) with the two green-colored U11/U12 di-snRNP densities shown in Figures 4A and 4B. These densities were therefore interpreted to be the SF3b49 RRMs; close-up views are shown in Figure 5A. The CCCs of these densities and the computed SF3b49 RRM models were 0.88 and 0.86 (Table S1), respectively, supporting this assignment of density to the SF3b49 RRMs.

The SF3b49 RRMs together with the ladder-like pattern of the first HEAT repeats and the two holes were used as a guide to fit the isolated SF3b into the U11/U12 di-snRNP. Independent confirmation of this location was provided by labeling experiments with antibodies (see below). The handedness of the U11/U12 di-snRNP determined by RCT was the same as that proposed on the basis of rigid-body fitting of isolated SF3b into the U11/U12 di-snRNP, thus providing an independent confirmation of handedness determined by RCT (see above).

A detailed comparison of the distribution of density around these anchor points (i.e., the first seven SF3b155 HEAT repeats, the holes, and the SF3b49 RRMs) in the two complexes suggested that the fit could be improved by a rotation of the SF3b49 RRMs with respect to the first seven HEAT repeats (Figure 4B). Indeed, a rotation of 20° resulted in an excellent fit of (1) the SF3b49 RRMs, (2) additional densities (a–c), and (3) one of the holes (red asterisks) to the density of U11/U12 di-snRNP.

Location of the Second Shell Half of Isolated SF3b in the U11/U12 di-snRNP

The structure of isolated SF3b resembles a closed bivalve shell. All of the SF3b anchor points identified in the U11/U12 di-snRNP are located in the same half of the SF3b shell. Thus, we next attempted to localize the second shell half of SF3b. In isolated SF3b, we found a kink in the HEAT repeat around tandem helix 7, which was considered to represent a potential hinge region; beyond this region, the repeats appeared to continue along a roughly circular path around the second shell half (Golas et al., 2003). A similar circularly ordered, ladder-like pattern is found in the side view of the outer wall of the U11/U12 di-snRNP (Figure 4C). Other structural features, including a central hole (Figure 4C, no. 13) and the peripheral contour (yellow dotted line), fit in well with this assignment. Furthermore, several elements of the structure are reminiscent of corresponding masses in the second shell half of isolated SF3b: these include (1) a horizontal density element (nos. 3 and 5) connected by a small bridge (no. 4) to the ladder-like repeats, (2) the right margins of the central hole (nos. 5 and 6), (3) a small protruding element on the right (no. 7), and (4) a sloped density at the bottom (nos. 8 and 9). Small variations in density are not unexpected because of differences in the resolution of the two structures. Indeed, certain fine-structural details of isolated SF3b appeared as more compact masses in the U11/U12 di-snRNP (compare nos. 12 and 14). However, variations appear in the lower left region in both complexes (white asterisks), the region previously proposed to represent a hinge.

Thus, we could determine the location not only of the first shell half of SF3b but also of the second shell half. The positions of the two SF3b shell halves were additionally confirmed by quantitative docking experiments that showed the highest CCCs with the shell half positions indicated in Figures 4 and 6. Significantly, compared with isolated SF3b, the two shell halves in the U11/U12 di-snRNP are in a more open conformation, suggesting a change in SF3b structure upon association with U11/U12 di-snRNPs (discussed in more detail below).

Additional Evidence for an SF3b Structural Rearrangement in U11/U12 di-snRNP

Additional evidence for a rearrangement in SF3b could be adduced by comparing the inner architecture of the two complexes. The U11/U12 di-snRNP has a diameter of ~135 × 150 Å in the region where SF3b was localized, as opposed to ~80 × 100 Å for isolated SF3b (Figure 6A). If SF3b in its isolated form were fitted directly into this region, a large density mismatch would result: a considerable amount of SF3b density would be located in regions of U11/U12 di-snRNP lacking such large masses (Figure 6A, orange asterisks). This interpretation is also supported by computing CCCs. By using the closed SF3b conformation, as found in isolated SF3b, a CCC of 0.24 was obtained, confirming the described density mismatch (Figure S6). By opening the two shell halves of SF3b, the CCC was increased to 0.71. To exclude a different orientation of the second SF3b shell half, we analyzed other fits found by a 3D alignment tool, but these all showed a lower correlation coefficient (0.48–0.58; Figure S6) making those orientations unlikely.

In summary, the data argue for an opening of SF3b upon its integration into the U11/U12 di-snRNP. This evidence includes (1) the direct observation of similar densities in isolated SF3b and U11/U12 di-snRNP (Figure 4C, numbered elements), (2) the obtained correlation maximum after fitting the second shell half into the

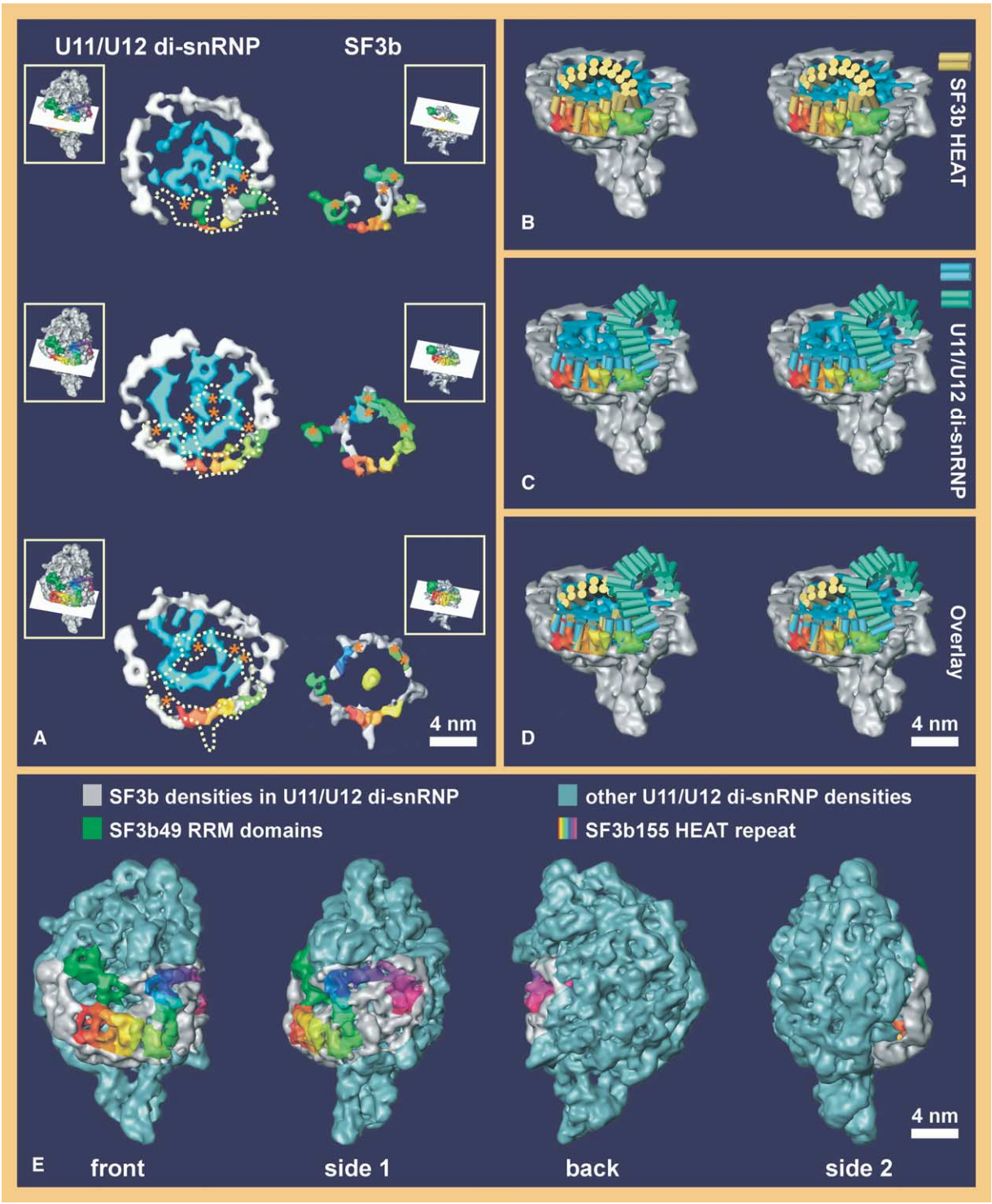

Figure 6. SF3b Densities in the U11/U12 di-snRNP

(A) Three sections of the U11/U12 di-snRNP (outer masses in silver, inner in blue) and SF3b (in silver, green for the SF3b49 RRMs, and rainbow colors for the SF3b155 HEAT repeat) are shown. The cutting planes are indicated by insets. The outline of SF3b is projected onto the section of the U11/U12 di-snRNP as a yellow dotted line. Comparison of the two structures supports the proposed rearrangement of SF3b into an open conformation during the assembly of the U11/U12 di-snRNP. The first rainbow-colored HEAT repeats show an excellent fit, whereas the inner densities of the U11/U12 di-snRNP reveal a substantial density mismatch with the isolated SF3b (orange asterisks) supporting a rearrangement of SF3b.

(B) To illustrate the movement of the second shell half of SF3b upon integration into the U11/U12 di-snRNP, the SF3b155 HEAT repeats found in the isolated SF3b (closed conformation) are depicted as golden double columns—each double column corresponding to one HEAT repeat. Orientation is provided by the bottom part of the U11/U12 di-snRNP in stereo view.

(C) Open conformation of the HEAT repeats found in the U11/U12 di-snRNP colored in blue (in front of the hinge) and green columns (behind the hinge).

(D) Overlay of the HEAT repeats found in isolated SF3b and the U11/U12 di-snRNP.

(E) Visualization of SF3b densities in the U11/U12 di-snRNP.

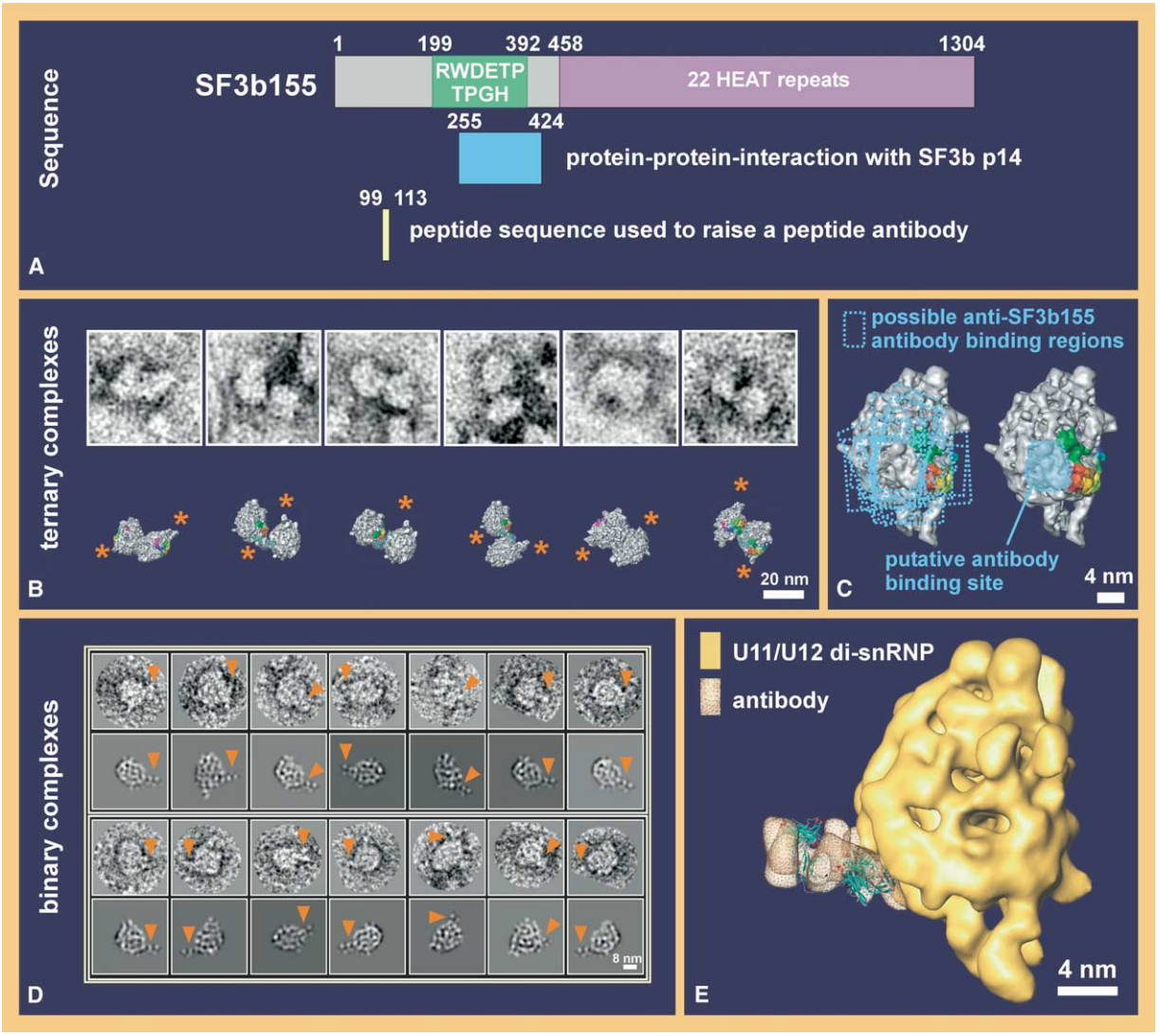

Figure 7. Anti-SF3b155 Antibody Labeling of U11/U12 di-snRNP

(A) Domain structure of the human SF3b155 protein (Wang et al., 1998).

(B) Ternary complexes. Selected and strongly lowpass-filtered images of the ternary complexes are shown above. The 3D surfaces of the U11/U12 di-snRNPs with a connecting antibody (Harris et al., 1998) are illustrated below. Asterisks mark the bottom of the U11/U12 di-snRNP.

(C) Localization of the anti-SF3b155 antibody in the ternary complexes. On the left side, regions of the U11/U12 di-snRNP where the two U11/U12 di-snRNPs are close enough to be candidates for the antibody binding site are marked by blue rectangles. On the right, the intersection of these possible binding sites is shown.

(D) Localization of the anti-SF3b155 antibody in binary complexes (150,000× magnification, 2-fold binned 1k × 1k CCD camera). In the first and third row, aligned particle images with bound antibody (orange arrowhead) are shown. Below each filtered image, the corresponding 2D reprojections (rows 2 and 4) are depicted.

(E) 3D representation of anti-SF3b155 antibody bound U11/U12 di-snRNPs and fitting of an antibody (PDB code: 1IGY, (Harris et al., 1998) into extra densities (brown) of the U11/U12 di-snRNP antibody complex. The anti-SF3b155 antibody interacts with the U11/U12 di-snRNP near the beginning of the HEAT repeats and in proximity to the interaction points of SF3b155 with p14 as expected from biochemical data.

shown density of the U11/U12 di-snRNP, and (3) a considerable density mismatch in the inner architecture of the U11/U12 di-snRNP when SF3b is fitted without the assumption of a conformational change (Figure 6A). This opening involves a rotation of one SF3b shell half by ~90° plus an additional small tilt in the hinge region around tandem helix 7. The structural differences are illustrated by the curvature of the HEAT repeats in a closed (Figure 6B) and open (Figure 6C) conformation of SF3b (overlay in Figure 6D; see also Movie S1). Due to this opening, most of the SF3b densities are accommodated in the bottom part of the U11/U12 di-snRNP (Figure 6E). Thus, the remaining U11/U12 di-snRNP components should be found in the upper third of the particle and extend down into the lower half. Large regions of density are found between the two SF3b shells, and these may represent interactions between SF3b and other U11/U12 di-snRNP components.

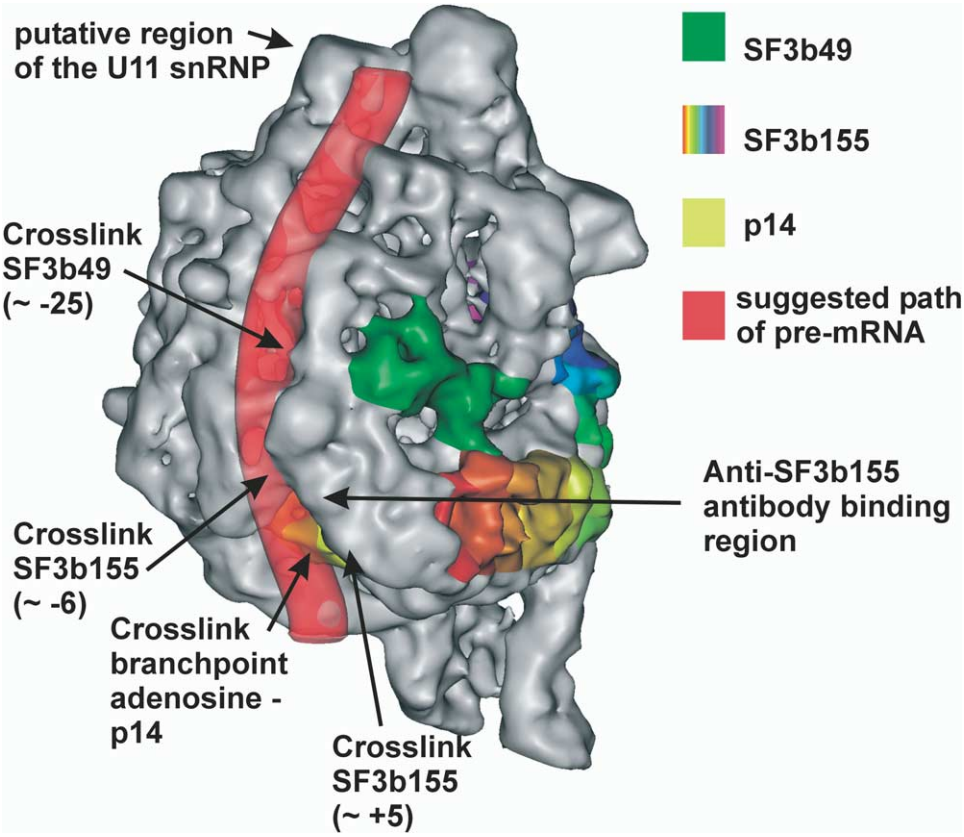

Figure 8. 3D Model of the Postulated Path of the pre-mRNA on the Surface of the U11/U12 di-snRNP

The model is based on previous crosslinking data and our structural interpretation of the U11/U12 di-snRNP (for details, see text).

Position of p14 within the U11/U12 di-snRNP

The location of p14 is important for functional interpretation, as this protein serves as a landmark for the spliceosome's active center. In isolated SF3b, p14 is located in the central cavity surrounded by an envelope (Golas et al., 2003) and is connected by two bridges to the SF3b regions that interact with the SF3b49 RRMs ([a]–[c] in Figure 4B). When parts of the SF3b densities are rotated to improve the fit of the SF3b49 RRMs into the U11/U12 di-snRNP (Figure 4B), p14 moves at the same time into a density element located on the outer surface of the U11/U12 di-snRNP. This location agrees well with the size (Figure S2B, density 3), mass (Figures S2B, S2C, and S3), and shape of an RRM without the need for postulating additional movement (Figure 5B). By using this location, a CCC of 0.97 for the RRM fit was obtained (Table S1), which was the highest of all putative RRM densities in the U11/U12 di-snRNP (Figures S5 and S8–S10).

Another density element adjacent to the putative p14 in U11/U12 di-snRNP also revealed some similarity to an RRM (Figure S7B). This density is located in the region where, according to the fit of the N-terminal HEAT repeats, one might expect to find p14 (Figures S7A–S7C). However, several observations suggested that this density is probably not p14. First, it is slightly too small (Figures S2B, S2C, and S3). Second, when the p14 RRM is fitted into this location, density corresponding to regions of the β sheet is partly missing (Figure S7D, arrows). This is also reflected by its lower CCC of 0.54. In summary, the most plausible location for p14 is on the outer surface of the U11/U12 di-snRNP.

Antibody Labeling of the U11/U12 di-snRNP

The localization of SF3b in the U11/U12 di-snRNP was based on the recognition of previously defined structural domains of SF3b by using characteristic features (size, mass, and CCC). To confirm the position of SF3b in the U11/U12 di-snRNP and provide additional evidence for the location of p14, immunolabeling studies were performed with an anti-SF3b155 antibody. This antibody binds to a region in proximity to the functionally important N terminus of the protein, which contains phosphorylation sites and the p14 binding site, and is located upstream of the N-terminal end of the HEAT motif (Figure 7A). Thus, the determination of the binding site of the anti-SF3b155 antibody allowed us to map independently the N-terminal end of the SF3b155 HEAT repeats and the approximate location of p14 within the U11/U12 di-snRNP.

To facilitate the analysis of antibody bound U11/U12 di-snRNPs, the latter were fractionated by glycerol-gradient centrifugation to separate binary complexes (i.e., one U11/U12 di-snRNP bound by one antibody) from ternary complexes (i.e., two U11/U12 di-snRNPs bound

by one antibody). For the binary complexes, 3D reconstruction was performed as described above. However, the conformational heterogeneity of ternary complexes precluded this kind of analysis, and thus, a two-dimensional (2D) analysis was performed.

Ternary Antibody Bound U11/U12 di-snRNP Complexes as Revealed by 2D Analysis

To determine the projection angle of the ternary complexes (Figure 7B, top), each particle of the ternary complex was masked manually, leaving only the density of one U11/U12 di-snRNP particle. All individual projection angles were determined by using exhaustive multireference alignment (MRA) via polar coordinates (Joyeux and Penczek, 2002; Sander et al., 2003b). For graphical evaluation, two copies of the U11/U12 di-snRNP structure were rotated by exactly these angles and shown as surface views including the antibody (Figure 7B, bottom). The U11/U12 di-snRNP pairs were found to be oriented in an almost antiparallel fashion, as one would expect when they are connected by an antibody. In Figure 7C (left), possible regions of the U11/U12–antibody interaction are marked for each U11/U12 di-snRNP in the ternary complexes by showing those regions of the particle that were close enough to be candidate antibody binding sites. The overlap area of all such individual putative binding regions therefore encloses the most plausible binding site of the antibody (Figure 7C, right). Accordingly, the SF3b155 antibody binding site is located at the bottom of the U11/U12 di-snRNP, close to the N-terminal end of the SF3b155 HEAT repeats.

Binary Antibody Bound U11/U12 di-snRNP Complexes as Revealed by 3D Analysis

In order to more precisely localize the antibody binding site, we determined the 3D structure of the binary complex (Figures 7D and 7E). As before, images were taken under two sets of conditions: (1) a high-contrast, low-resolution control (magnification: 150,000× and CCD camera) and (2) a higher-resolution data set (magnification: 50,000×, film, and cryo conditions). Figure 7D shows class averages (first and third row) and reprojections (second and fourth row); the antibody is visible as an extended region of density (orange arrows). In the 3D map, the antibody was shown to bind close to one of the holes found above the HEAT repeats, defining the beginning of the SF3b155 HEAT motif (left-hand hole in Figure 2D; the bound antibody is shown in Figure 7E). A major portion of the antibody density was visible in the 3D map. However, parts of the antibody—such as the connecting loops between the β strands of the immunoglobulin domains of the antibody—are not seen, owing to the flexibility of the antibody. Furthermore, the Fc and unbound Fab fragment are also less clearly seen.

Remarkably, the antibody binding site is close to the points at which p14 is connected to the SF3b outer shell with the N-terminal SF3b155 HEAT repeats as suggested both by biochemical data and by our interpretation. Protein–protein interaction studies have shown that p14 interacts with aa 255–424 of SF3b155 (Will et al., 2001). The antibody used in the present study was raised against a sequence corresponding to aa 99–113 of SF3b155 (Figure 7A). Therefore, the spatial proximity between the anti-SF3b155 antibody binding site and the densities connecting p14 to the rest of the SF3b particle, as well as its proximity to the SF3b155 HEAT motif, agree well with published biochemical data.

Discussion

Architecture of the Spliceosomal U11/U12 di-snRNP

We describe here the 3D structure of human U11/U12 di-snRNP and the location of some of its major structural elements. To determine this structure, we have applied two different approaches: (1) angular reconstitution and (2) RCT. These two independent methods revealed a similar structure, supporting the correctness of the 3D reconstructions. At the level of resolution obtained by angular reconstitution, the pattern of SF3b155 HEAT repeats and the RRM domains of SF3b49 and p14 were located within the U11/U12 di-snRNP. Anti-SF3b155 antibody labeling independently supported this assignment as the antibody bound in spatial proximity to the N-terminal end of the HEAT repeats. These data played a crucial role in the localization of the entire SF3b within the U11/U12 di-snRNP. The structural comparison between the U11/U12 di-snRNP and isolated SF3b furthers our understanding of splicing at the molecular level and provides insights into the architecture of early spliceosomal complexes.

Identification of Structural Domains in the U11/U12 di-snRNP

Several proteins of the U11/U12 di-snRNP contain known structural domains, including HEAT, RRM, and Sm domains. SF3b155 is predicted to possess 22 tandem-helical HEAT repeats (Wang et al., 1998). At the resolution of the U11/U12 di-snRNP, the most regular parts of the HEAT motif were identified as separated columns, each consisting of two antiparallel helices. Antibody labeling with an antibody recognizing an epitope in some proximity to the N-terminal end of the SF3b155 HEAT repeats and the p14 interaction site independently confirmed this localization. The remaining HEAT repeats appeared as a semicircular ladder-like pattern in the side view of the U11/U12 di-snRNP. This pattern was essential for identifying the second shell half within the U11/U12 di-snRNP. Geometrical considerations and analysis of the CCCs calculated for different conformations provided additional support.

Several U11/U12 di-snRNP proteins contain RRM domains. These proteins include SF3b49, p14, 65K, 35K, 31K, and Urp (Champion-Arnaud and Reed, 1994; Will et al., 2001, 2004). In the 3D map, we found at least 11 putative RRM domains, the sizes and shapes of which agreed with those of an RRM. In isolated SF3b, all three identified RRMs belong to the same shell half. Thus, upon moving shell halves with respect to each other, the relative orientation of the RRMs should remain very similar to that found in isolated SF3b. SF3b49 is predicted to be the only U11/U12 di-snRNP protein with two adjacent RRMs. U11/U12-65K also possesses two RRMs, but they are separated by a long stretch of amino acids and are thus unlikely to be adjacent to one another (Will et al., 2004). CCCs of SF3b49

RRM densities extracted from isolated SF3b with putative adjacent RRM domains in the U11/U12 di-snRNP revealed the best fit for those two densities located above the left hole in the frontal view and were thus assigned to the SF3b49 RRMs, similar to the isolated SF3b. The p14 RRM that is connected to densities interacting with SF3b49 in isolated SF3b appears to be located on the surface of the U11/U12 di-snRNP. An adjacent putative RRM-like mass could be excluded as p14 because of differences in size, a lower CCC, and a density mismatch for part of the p14 β sheet. Furthermore, the U11/U12 di-snRNP can be immunoprecipitated by an anti-p14 antibody directed against the C terminus of p14 (Will et al., 2001), indicating that this region of p14 is accessible. In the illustrated location (Figure 5B), p14 is found in the outer region of the U11/U12 di-snRNP, thereby allowing an interaction with antibody. However, in the position of the alternative RRM-like mass, p14 would be located in the inner densities of the U11/U12 di-snRNP and would thus hardly be accessible to an antibody. Attempts to locate p14 directly in the U11/U12 di-snRNP by using the p14 antibody failed due to insufficient antibody bound particles. The remaining putative RRM domains were not assigned to specific U11/U12 di-snRNP proteins, owing to the lack of additional structural and/or biochemical data about these proteins.

Similar limitations apply to the identification of the two Sm cores in the U11/U12 di-snRNP. The 3D structure of a complete Sm ring in the U1 snRNP that consists of the U1 snRNA, the Sm proteins, and three particle-specific proteins shows an asymmetric funnel-like shape (Stark et al., 2001). In larger macromolecular complexes such as the U11/U12 di-snRNP, it is not unlikely that the Sm cores might be distorted or occluded by direct interactions with other snRNP components, making their localization difficult.

Structural Basis for the Interaction of p14 and the Branchpoint Adenosine of the pre-mRNA

The 3D structure of isolated SF3b showed p14 to be enclosed within an envelope (Golas et al., 2003). Access to the interior of SF3b is only possible through small openings in the envelope of SF3b. However, crosslinking studies demonstrated a direct interaction between p14 and the branchpoint adenosine (Query et al., 1996; Will et al., 2001), raising the question of how this apparent steric problem might be solved. In general, there are two possibilities enabling an interaction between p14 and the branch site. In the first, the pre-mRNA would be threaded through the openings of SF3b. However, the latter appear to be too small to allow the entry of folded, protein bound pre-mRNA into the inner cavity of SF3b. Therefore, this model would require conformational changes in the protein bound pre-mRNA, including changes in the tertiary structure of the pre-mRNA or the stripping off of proteins from the pre-mRNA. In the second model, SF3b would undergo structural changes in which its conformation would be opened to allow direct access of pre-mRNA to p14.

By comparing the 3D structure of the native U11/U12 di-snRNP with its isolated subcomplex SF3b, an answer to this fundamental and functionally relevant question of p14-branchpoint interaction was obtained. During the assembly of the U11/U12 di-snRNP, SF3b adopts a more open conformation, leading to the exposure of p14 to the solvent. This conformation allows direct interaction of p14 with the pre-mRNA, without the assumption of additional conformational changes. Whether the opening of SF3b takes place during the assembly of the U12 snRNP or in a later step during formation of the U11/U12, di-snRNP is currently unclear. Additional studies of earlier assembly stages might be instrumental in answering this question.

Model for the Structural Rearrangements of Isolated SF3b upon Integration into the U11/U12 di-snRNP

Our data reveal different curvatures of the HEAT repeats in isolated SF3b and in the U11/U12 di-snRNP. Comparison of these curvatures suggests a rearrangement of SF3b into an open conformation upon integration into the U11/U12 di-snRNP. The proposed movement of the two shell halves can be described by a ~90° rotation plus an additional small tilt around the hinge region at helix pair 7. The overall conformation of the HEAT repeats in front of and behind the hinge region remains largely unchanged.

An important question is how such a conformational change might be accomplished. A likely candidate domain that drives this rearrangement might be the SF3b155 HEAT motif itself, as it spans both shell halves of SF3b and connects them in the hinge region (Golas et al., 2003). This idea is supported by the observation of changes in the curvature of the HEAT repeats in other proteins, such as importin-β upon binding to one of its interaction partners, importin-α or Ran (Cingolani et al., 1999; Vetter et al., 1999).

The suggested opening of the two shell halves of SF3b is necessarily coupled to a dissociation of protein–protein interactions within SF3b. DEAD-box RNA helicases may possess RNPase function (Fairman et al., 2004; Jankowsky et al., 2001) capable of remodeling RNA-protein complexes by ATP hydrolysis. The newly discovered DEAD-box protein SF3b125 (Will et al., 2002) represents a good candidate for involvement in this proposed SF3b remodeling.

Model for the Interactions between U11/U12 di-snRNP and pre-mRNA

On the basis of (1) previous crosslinking data, (2) the locations of SF3b49 and SF3b155, (3) immunolabeling of SF3b155, and (4) the suggested interaction of p14 with the branchpoint adenosine on the surface of the U11/U12 di-snRNP, a model for the putative path of the pre-mRNA bound to the U11/U12 di-snRNP can be proposed (Figure 8), assuming similar SF3b/pre-mRNA interactions in the minor and major spliceosome. SF3b49, SF3b145, SF3b155, and p14 have been crosslinked to the branchpoint region of the pre-mRNA in the major spliceosome (Champion-Arnaud and Reed, 1994; Gozani et al., 1996, 1998; Query et al., 1996). Parts of the SF3b155, SF3b49, and p14 proteins are oriented, in proximity to one another, in a straight line on the surface of U11/U12 di-snRNP. The pre-mRNA would thus fit nicely into a long groove on the U11/U12 di-snRNP surface that connects the bottom part of the U11/U12 di-snRNP, comprising SF3b densities and the top of the U11/U12 di-snRNP. Interestingly, this top region of the U11/U12 di-snRNP is composed of elements that resemble the U1 snRNP (Stark et al., 2001), and thus possibly represent the U11 snRNP.

In contrast to its major spliceosomal counterparts—U1 and U2 snRNP—the preformed U11/U12 di-snRNP binds cooperatively to the 5′ splice site and the branchpoint re-

gion of the intron (Frilander and Steitz, 1999). The proposed path of the pre-mRNA in a longitudinal groove might therefore provide the morphological basis for this strong cooperativity at the 3D level, as binding of the pre-mRNA to one point of this groove should facilitate binding to other regions of the groove. In conclusion, the U11/U12 di-snRNP represents a key structure for the understanding of the structural dynamics of early spliceosomal complexes and provided first insights into their structural organization.

Experimental Procedures

Isolation of Native U11/U12 di-snRNP

Spliceosomal snRNPs were isolated from HeLa nuclear extract by anti-m^3G affinity chromatography and were fractionated on a glycerol gradient (10%–30%). The 18S gradient peak (250 mM KCl) was incubated with a biotinylated 2′O-methyl-oligonucleotide (5′-AUUUUCCUUACU CAUAAGdTdTdTdT-3′) directed against nucleotides 11–28 of the U12 snRNA for 16 hr at 4°C and subsequently incubated with streptavidin agarose (Will et al., 1999). After washing briefly with ETO buffer (1 mM Hepes [pH 7.9], 0.25 mM EDTA, 0.5 mM DTE, 0.02% Tween 20, and 5% glycerol), the particles were eluted twice in ETO buffer by incubating at 37°C for 7.5 min, and the salt concentration was adjusted to 150 mM. The RNA and protein compositions were analyzed on a 10% polyacrylamide/7 M urea gel and on a 10%/13% polyacrylamide/SDS gel, respectively.

Antibody Labeling of U11/U12 di-snRNP

Before elution, streptavidin bound U11/U12 di-snRNPs were incubated for 2 hr at 4°C with an affinity-purified rabbit antibody directed against SF3b155 (aa 99–113; Will et al., 2001) for 2 hr at 4°C. After washing extensively, U11/U12 di-snRNPs were eluted as described above, except the salt concentration was adjusted to 50 mM. The sample was subsequently concentrated four to five times in a vacuum desiccator. Antibody bound U11/U12 di-snRNP exhibited a slightly faster sedimentation behavior as compared to unbound U11/U12 di-snRNPs. Very few antibodies interacted with two U11/U12 di-snRNPs.

Sample Preparation for Electron Microscopy

U11/U12 di-snRNP particles (~20 μg/ml) were adsorbed onto a small piece of carbon film. The film was transferred to a well filled with 2% uranyl formate in water and incubated for 2 min. The carbon film was lifted from the staining solution with an electron microscopy (EM) grid covered with a perforated carbon film. A second carbon film floated in another well containing 2% uranyl formate was placed on top of the first film. After blotting, the grid was stored either at room temperature or in liquid nitrogen. To assess the risk of obtaining positive staining of RNA by this method, 50S ribosomal subunits were examined as a control (M.M.G., B.S., and H.S., unpublished data). The structure was compared with a 3D map of 50S ribosomes obtained by native cryo-EM. No significant differences within the resolution limit of the reconstructions were seen.

High-Contrast EM of U11/U12 di-snRNP on a CCD Camera

We used a Philips CM200 FEG electron microscope at a magnification of 150,000× with a defocus of 2.8–4.2 μm at 200 kV. Images were taken at room temperature on a 2-fold binned 1k × 1k CCD camera (TVIPS, Gauting, Germany), resulting in sampling of 48 × 48 μm. The electron dose was ~30/Å^2. 2352 particles were selected interactively and CTF corrected (Sander et al., 2003a).

High-Resolution EM of the U11/U12 di-snRNP on Film

A Philips CM200 FEG operated at 160 kV and at a magnification of 38,000× with a Gatan cryo-holder was used for EM investigation under low-dose conditions (~15–20 electrons/Å^2). Images were taken at defoci of 1.5–2.5 μm on Kodak SO-163 film and were scanned with a rotating-drum scanner (Tango, Heidelberger Druckmaschinen, Germany) at a step size of 4 μm (1.05 Å pixel size). For initial calculations, the images were binned by a factor of four. About 9000 particles were interactively selected and CTF corrected. Low-quality images were excluded, leaving the best 8756 particles.

EM of Antibody-Labeled U11/U12 di-snRNP

Particles were imaged by using a Philips CM200 operated at 200 kV (~15–20 electrons/Å^2), a defocus of 0.59–2.34 μm, and a magnification of 50,000× on Kodak SO-163 film at liquid nitrogen temperature. Images were scanned (Tango) at 1200 dpi (4.2 Å pixel size). About 2500 binary particles were selected manually and corrected for the CTF. Similarly, ternary complexes were selected manually. Another data set, for higher contrast, was imaged at a magnification of 150,000× by using a 1k × 1k CCD camera binned to 512 × 512 pixels (~30 electrons/Å^2) at room temperature. 3689 particles were selected manually and corrected for the CTF.

Random Conical Tilt

760 particles were imaged at a magnification of 150,000× and a defocus of ~4 μm first with a tilt of 37.5° and afterwards at a tilt of 0°. Images were taken on a 1k × 1k CCD camera binned to 512 × 512 pixels (~30 electrons/Å^2). Particles were selected manually from the untilted and from the corresponding tilted images. Untilted images were aligned by using iteratively refined class averages as references and subsequent MSA for classification into ten classes. Angles of the tilted images of the five largest classes were determined according to Radermacher (1988). A 3D map was calculated independently for each class, and an average 3D of the five largest classes was obtained after 3D alignment of individual 3D structures by using the 3D alignment tool of the software AmiraDev 2.3 (TGS Europe, Merignac Cedex, France).

Angular Reconstitution

The single particle averaging method was employed in the context of IMAGIC-5 (van Heel et al., 1996). Class averages with improved signal-to-noise ratio were obtained after MRA, MSA, and classification. Angles of class averages were determined by angular reconstitution (van Heel, 1987). Several subsequent rounds of iterative projection matching refinements using corrim–based MRA via polar coordinates (Sander et al., 2003b) were used to compute the final 3D map. The resolution of the final 3D reconstruction was determined by the FSC function (Harauz and van Heel, 1986).

Visualization of the U11/U12 di-snRNP Structure and Fitting of SF3b Densities into the U11/U12 di-snRNP

Surface representations were visualized with AmiraDev 2.3. For fitting using the 3D alignment tool, the SF3b densities were cut into three parts: (1) front helices and surrounding densities; (2) SF3b49 RRMs, p14, and intervening masses; and (3) the second half of the "bivalve" shell harboring most of the HEAT repeats. Previously computed RRM models of SF3b49 and p14 (described in Golas et al. [2003]) as well as of 65K, 35K, 31K, and Urp created by Swiss-Model (Schwede et al., 2003) were used for fitting. Fittings were performed manually and by the software Situs (Wriggers and Birmanns, 2001). Normalized CCCs were calculated for all fits.

Analysis of Antibody Labeling Using Ternary Complexes

Ternary complexes were masked manually to obtain two separate U11/U12 di-snRNP particles. Angles of each particle were determined by projection matching using exhaustive MRA via polar coordinates (Sander et al., 2003b). Surface representations of the U11/U12 di-snRNP were rotated according to the angles and were connected by an antibody for presentation purposes (pdb code, 1IGY; Harris et al., 1998).

Visualization of Antibody Bound U11/U12 di-snRNP

The 3D structure of antibody bound U11/U12 di-snRNP was calculated as described above. Extra masses due to the antibody were analyzed in two dimensions (single images and class averages) and in three dimensions (3D reconstruction). Initial alignment references were created from the lowpass-filtered 3D map of U11/U12 di-snRNP. The 3D structure of an antibody was used to dock it man-

ually into the additional densities of the antibody bound U11/U12 di-snRNP.

Supplemental Data

Supplemental Data include a Supplemental Summary, one movie, ten figures, and one table and are available with this article online at http://www.molecule.org/cgi/content/full/17/6/869/DC1/.

Acknowledgments

We thank Gabi Heyne for expert technical assistance. This work was supported by grants from the Federal Ministry of Education and Research, Germany to R.L. and H.S. (031U215B), the Deutsche Forschungsgemeinschaft to R.L. (LU294/12-1), and the Fonds der chemischen Industrie to R.L.

Received: October 15, 2004
Revised: December 23, 2004
Accepted: February 14, 2005
Published: March 17, 2005

References

Burge, C.B., Tuschl, T., and Sharp, P.A. (1999). Splicing of precursors to mRNAs by the spliceosomes. In The RNA World, Second Edition, R.F. Gesteland, T.R. Cech, and J.F. Atkins, eds. (Cold Spring Harbor, NY: Cold Spring Harbor Laboratory Press), pp. 525–560.

Champion-Arnaud, P., and Reed, R. (1994). The prespliceosome components SAP 49 and SAP 145 interact in a complex implicated in tethering U2 snRNP to the branch site. Genes Dev. *8*, 1974–1983.

Cingolani, G., Petosa, C., Weis, K., and Müller, C.W. (1999). Structure of importin-beta bound to the IBB domain of importin-alpha. Nature *399*, 221–229.

Das, B.K., Xia, L., Palandjian, L., Gozani, O., Chyung, Y., and Reed, R. (1999). Characterization of a protein complex containing spliceosomal proteins SAPs 49, 130, 145, and 155. Mol. Cell. Biol. *19*, 6796–6802.

Fairman, M.E., Maroney, P.A., Wang, W., Bowers, H.A., Gollnick, P., Nilsen, T.W., and Jankowsky, E. (2004). Protein displacement by DExH/D "RNA helicases" without duplex unwinding. Science *304*, 730–734.

Frilander, M.J., and Steitz, J.A. (1999). Initial recognition of U12-dependent introns requires both U11/5′ splice-site and U12/branchpoint interactions. Genes Dev. *13*, 851–863.

Golas, M.M., Sander, B., Will, C.L., Lührmann, R., and Stark, H. (2003). Molecular architecture of the multiprotein splicing factor SF3b. Science *300*, 980–984.

Gozani, O., Feld, R., and Reed, R. (1996). Evidence that sequence-independent binding of highly conserved U2 snRNP proteins upstream of the branch site is required for assembly of spliceosomal complex A. Genes Dev. *10*, 233–243.

Gozani, O., Potashkin, J., and Reed, R. (1998). A potential role for U2AF-SAP 155 interactions in recruiting U2 snRNP to the branch site. Mol. Cell. Biol. *18*, 4752–4760.

Harauz, G., and van Heel, M. (1986). Exact filters for general geometry three-dimensional reconstruction. Optik *73*, 146–156.

Harris, L.J., Skaletsky, E., and McPherson, A. (1998). Crystallographic structure of intact IgG1 monoclonal antibody. J. Mol. Biol. *275*, 861–872.

Jankowsky, E., Gross, C.H., Shuman, S., and Pyle, A.M. (2001). Active disruption of an RNA-protein interaction by a DExH/D RNA helicase. Science *291*, 121–125.

Joyeux, L., and Penczek, P.A. (2002). Efficiency of 2D alignment methods. Ultramicroscopy *92*, 33–46.

Krämer, A., Grüter, P., Gröning, K., and Kastner, B. (1999). Combined biochemical and electron microscopic analyses reveal the architecture of the mammalian U2 snRNP. J. Cell Biol. *145*, 1355–1368.

MacMillan, A.M., Query, C.C., Allerson, C.R., Chen, S., Verdine, G.L., and Sharp, P.A. (1994). Dynamic association of proteins with the pre-mRNA branch region. Genes Dev. *8*, 3008–3020.

Patel, A.A., and Steitz, J.A. (2003). Splicing double: insights from the second spliceosome. Nat. Rev. Mol. Cell Biol. *4*, 960–970.

Query, C.C., Strobel, S.A., and Sharp, P.A. (1996). Three recognition events at the branch-site adenine. EMBO J. *15*, 1392–1402.

Radermacher, M. (1988). Three-dimensional reconstruction of single particles from random and nonrandom tilt series. J. Electron Microsc. Tech. *9*, 359–394.

Sander, B., Golas, M.M., and Stark, H. (2003a). Automatic CTF correction for single particles based upon multivariate statistical analysis of individual power spectra. J. Struct. Biol. *142*, 392–401.

Sander, B., Golas, M.M., and Stark, H. (2003b). Corrim-based alignment for improved speed in single particle image processing. J. Struct. Biol. *143*, 219–228.

Schwede, T., Kopp, J., Guex, N., and Peitsch, M.C. (2003). SWISS-MODEL: An automated protein homology-modeling server. Nucleic Acids Res. *31*, 3381–3385.

Stark, H., Dube, P., Lührmann, R., and Kastner, B. (2001). Arrangement of RNA and proteins in the spliceosomal U1 small nuclear ribonucleoprotein particle. Nature *409*, 539–542.

van Heel, M. (1987). Angular reconstitution: a posteriori assignment of projection directions for 3D reconstruction. Ultramicroscopy *21*, 95–100.

van Heel, M., Harauz, G., and Orlova, E.V. (1996). A new generation of the IMAGIC image processing system. J. Struct. Biol. *116*, 17–24.

Vetter, I.R., Arndt, A., Kutay, U., Görlich, D., and Wittinghofer, A. (1999). Structural view of the Ran-Importin beta interaction at 2.3 A resolution. Cell *97*, 635–646.

Wang, C., Chua, K., Seghezzi, W., Lees, E., Gozani, O., and Reed, R. (1998). Phosphorylation of spliceosomal protein SAP 155 coupled with splicing catalysis. Genes Dev. *12*, 1409–1414.

Will, C.L., Schneider, C., Reed, R., and Lührmann, R. (1999). Identification of both shared and distinct proteins in the major and minor spliceosomes. Science *284*, 2003–2005.

Will, C.L., Schneider, C., MacMillan, A.M., Katopodis, N.F., Neubauer, G., Wilm, M., Lührmann, R., and Query, C.C. (2001). A novel U2 and U11/U12 snRNP protein that associates with the pre-mRNA branch site. EMBO J. *20*, 4536–4546.

Will, C.L., Urlaub, H., Achsel, T., Gentzel, M., Wilm, M., and Lührmann, R. (2002). Characterization of novel SF3b and 17S U2 snRNP proteins, including a human Prp5p homologue and an SF3b DEAD-box protein. EMBO J. *21*, 4978–4988.

Will, C.L., Schneider, C., Hossbach, M., Urlaub, H., Rauhut, R., Elbashir, S., Tuschl, T., and Lührmann, R. (2004). The human 18S U11/U12 snRNP contains a set of novel proteins not found in the U2-dependent spliceosome. RNA *10*, 929–941.

Wriggers, W., and Birmanns, S. (2001). Using situs for flexible and rigid-body fitting of multiresolution single-molecule data. J. Struct. Biol. *133*, 193–202.

Accession Numbers

The density map of the U11/U12 di-snRNP has been deposited at the Macromolecular Structure Database under accession number EMD-1096.